This article has been accepted for publication in a future issue of this journal, but has not been fully edited. Content may change prior to final publication. Citation information: DOI 10.1109/JLT.2016.2518921, Journal of Lightwave Technology

Human Immunoglobulin Class G (IgG) Antibody Detection with Photonic Crystal Fiber

Jad Rabah, Alpha Mansaray, Rosalind Wynne, *Member, IEEE,* and Metin Duran

***Abstract*—Dye-free antibodies were identified in a less than 5nL volume with a solid-core photonic crystal fiber (SC-PCF). The all-silica fiber contained micron sized features with a 3 μm diameter core supported by a steering wheel shaped lattice. These structures can be employed to monitor the presence of immunobased assays and susceptible secondary antigens specific to the detection application. A 0.8 m section of SC-PCF was filled with a 4.47 nL antibody sample and a LED light source in the 1300 nm -1700 nm range was employed. Although similar sensing configurations exist, the novelty of this investigation is the detection of this particular antibody. This experiment uniquely investigates the spectral characteristics of purified human immunoglobulin class G (IgG) (format-UNLB) in aqueous media. The absorption spectra for the mAbs were collected with a conventional optical spectrum analyzer. The antibody solution exhibited two distinct absorption peaks, a water linked absorption peak between 1400 nm and 1470 nm, with a maximum absorption power of 1.65 nW, and an antibody linked absorption peak between 1485 nm and 1590 nm with a maximum absorption power of 3.2 nW.**

***Index Terms*—microstructured optical fibers, absorption spectroscopy, antibody detection.**

I. Introduction

AN antibody is a large protein that is used to identify a unique part of a target, called the antigen. It uses a lock-key mechanism where the antibody has a lock that binds to a specific key in the targeted cell. Monoclonal antibodies, or mAbs, are classically defined as specific antibodies that are produced by a homogeneous set of immune cells, which are exact genetic copies of an original parent cell. In this article, a more liberal and commonly accepted definition of mAbs is invoked [1]. Here the term monoclonal antibodies includes antibodies containing a single antibody recognizing only a single determinant, i.e., antigen. Monoclonal antibodies characteristically bind to the same specific piece of antigen using a lock-key mechanism. They are an important tool in identifying and purifying substances.

This article describes a label-free mAb sensor using absorption spectroscopy. The importance of having a portable mAb sensor is broadly supported and demonstrated in widespread applications [2]. Compact antibody detection systems that do not require sample preprocessing are especially attractive. For example, biohazard detection is important to the medical, environmental pollution monitoring, food safety and industrial process control industries. Portable monitoring systems are suitable for point-of-care testing that provides real-time monitors for components like blood glucose, fertility hormones and cardiac stress proteins. Previous studies have investigated the monitoring of biomolecules with photonic crystal fiber. Such investigations include the detection of enzymes [3], proteins, antigens and antibodies labeled with fluorescent dyes [4] and quantum dots [5], [6]. These previous reports have demonstrated similar sensing configurations however, they do not include the label-free detection of this particular antibody. Label-free methods of biomolecule detection have also been documented [7], [8], [9].

Other label-free biosensors have demonstrated high sensitivities [10], [11]. In [10], an As_2S_3 chalcogenide tapered fiber was designed for the detection of biomolecules. In this numerical investigation, the biomolecules modulates the thickness of the antigen-antibody layer coating the tapered region to directly affect the fiber dispersion. The sensor exploits the fundamental nonlinear process of modulation instability or degenerate four wave mixing. A record sensitivity of $\sim$ 18nm/nm (shift in resonance wavelength per nanometer biolayer thickness) was predicted for this design. Other high-sensitivity biosensor design configurations based on a dual-core microstructured polymer optical fibers (mPOF) also offer label-free detection. In [11] numerical investigations produced notable sensitivities of 20nm/nm (shift in resonance wavelength per nanometer biolayer) for the detection of α-streptavidin while operating at wavelengths in the visible regime. The report describes antibody molecules captured by an antigen layer in a mPOF air-hole such that the antibody-antigen layer thickness modifies the coupling length between neighboring cores.

The conventional method for mAb detection is Enzyme-Linked Immunosorbent Assay (ELISA). Antibody detection using ELISA involves several steps that include washes and incubation periods that may take up to a day each, and need to be performed by a highly skilled staff [2].

This article discusses absorption spectroscopy in the near infrared range employing a photonic crystal fiber as a sensing platform. Absorption spectroscopy is an analytical procedure that quantitatively determines the constituents and composition of an aqueous or gaseous mixture, or the presence of a specific analyte in a sample [12]. The findings presented in this article provide an in-depth investigation of questions that surfaced during preliminary investigations of mAb detection [13], [14]. In that previous study, the high concentration of mAb samples were in a buffer solution which limited analysis of the absorption signature. Here the buffer interference of the mAb signature was avoided using a lower concentration and

R. Wynne is with the Department of Electrical and Computer Engineering, Villanova University, Villanova, PA, 19085 USA e-mail: (rosalind.wynne@villanova.edu).

Manuscript received September 19, 2015; revised December 30, 2015.

0733-8724 (c) 2015 IEEE. Personal use is permitted, but republication/redistribution requires IEEE permission. See http://www.ieee.org/publications_standards/publications/rights/index.html for more information.

This article has been accepted for publication in a future issue of this journal, but has not been fully edited. Content may change prior to final publication. Citation information: DOI 10.1109/JLT.2016.2518921, Journal of Lightwave Technology

less than 10 nL sample volumes. The primary interest for this investigation was to achieve reduced sample preparation times and to reduce acquisition (i.e. sample filling) rates. The limited sample volumes and filling times occurred at the expense of enhanced sensitivities that are provided by long interaction lengths.

An overview of absorption spectroscopy principles is discussed in section II. In section III, a detailed review of solid core photonic crystal fiber (SC-PCF) is discussed. SC-PCF provides a novel approach to mAb sensing. Sections IV and section V contain the sensor design and development, including the experimental configuration, the mAb analyte preparation, and the measured results that demonstrate mAb absorption. The conclusion is presented in Section VI.

II. Absorption Spectroscopy

Absorption spectroscopy is the spectroscopic analysis of the absorption of energy from a radiating field. It is presented in this article as a function of wavelength, characteristic to the absorption of the field by the material [15], [16], [17]. It is an analytical tool in determining the presence and quantity of substances in a sample. An absorption spectrum is governed by the fraction of absorbed radiation by the substance in a range of wavelengths. The absorption spectrum might also depend on the structure of the molecules, and on environmental conditions such as temperature, pressure and electromagnetic field, which will alter the width and shape of the absorption spectrum.

1) Absorption Spectroscopy Principles: Light traveling through a material will encounter many processes including absorption [12], [18]. The Beer-Lambert law describes the principles of linear absorption of light by a specific medium [12]. This relationship is valid for the case of an optical field of intensity I_z traveling in the z direction of a medium of a particular concentration. The absorption term is α if no scattering is assumed. When a polychromatic light source is being used in the detection method, it is convenient to express the Beer-Lambert law in the following form $I = I_0 \exp(-\alpha z)$.

2) Practical Considerations: Practical absorption profiles exhibit a broadened linewidth influenced by a number of mechanisms. Absorption characteristics can suffer distortions in practice that can be influenced by three main broadening mechanisms: the Doppler effect, molecular collisions and transit time effects [19], [20]. Broadening can be compounded by collisions with the inner walls of the sample housing. In the specific case of SC-PCF fibers used in this article, the wall collisions are significant due to the small 22 μm diameter. The theory behind spectral absorption and the primary broadening phenomena have been qualitatively and mathematically described [19], [18], [21], [22]. In practice, the spectra can be represented by a Voigt profile which captures the combined broadening effects.

III. Solid Core Photonic Crystal Fiber

The classification of PCF used in this article is solid-core photonic crystal fiber (SC-PCF) shown in Fig. 1. The steering wheel photonic crystal fiber (SW-PCF) is a SC-PCF fiber that has a solid core with 3 surrounding hollow channels and 3 webbings supporting the core, giving the cross section of the fiber a steering wheel look. This type of PCF was chosen due to the advantages of its unique structure. It has three large air holes that enhance the transportation of the host sample into the structure, hence improving the ease of use. The small core causes optical power coupling into the holes, thus providing a significant mode-air overlap without reducing the outer cladding diameter of the fiber and therefore structural integrity is not sacrificed. This kind of core structure enhances the intensity and the overlap of the evanescent wave, which is a highly desirable characteristic for evanescent field sensing applications [23].

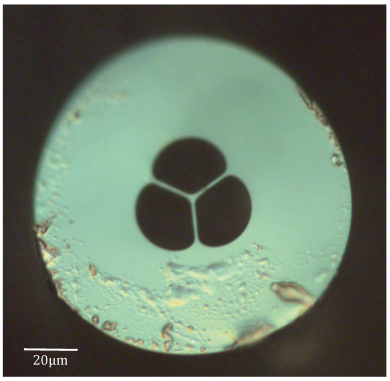

Fig. 1. A cross-section of a steering wheel photonic crystal fiber is shown.

The solid core diameter of the PCF is 3.3 μm, while the microstructure air-hole is 22 μm as shown in Fig. 1. The larger surface area allows aqueous samples to coat the internal structure of the fiber which promotes increased sensitivity. The aqueous sample can be detected via the evanescent field [24].

A. Attenuation

Any attenuation by the fiber is critical to this application and tests were performed to confirm the attenuation spectrum specified by the fiber manufacturer which cites strong attenuation in the 1350 nm to 1450 nm region. A baseline was taken by connecting a Hewlett Packard model 83437A LED light source to a Yokogawa model AQ6370 spectrum analyzer via a single mode fiber, then a piece of 0.8 m SW-PCF fiber was coupled to the broadband LED and to the spectrum analyzer in the same manner. The transmission characteristics agrees with the manufacturer specifications, having strong attenuation (0.3dB/m) near 1380 nm [23].

The core is relatively very small such that the fundamental mode distribution extends out to the large air holes that surround the core. The mode distribution is dependent on the diameter of the air holes of the PCF at a particular wavelength. This mode leak into the air holes, which will eventually house the sample, is the basis of the sensing technique. As the mode diameter increases, the interaction between the evanescent wave and the sample increases, enhancing the accuracy of the sensor.

Longer wavelengths lead to larger portions of the fundamental core mode intensity coupling into the air holes. This is due

0733-8724 (c) 2015 IEEE. Personal use is permitted, but republication/redistribution requires IEEE permission. See http://www.ieee.org/publications_standards/publications/rights/index.html for more information.

This article has been accepted for publication in a future issue of this journal, but has not been fully edited. Content may change prior to final publication. Citation information: DOI 10.1109/JLT.2016.2518921, Journal of Lightwave Technology

to the increase in effective indices and decrease in effective non-linearities as the wavelength increases [23]. At 1500 nm, the steering wheel photonic crystal fiber has been calculated to have a mode intensity overlap of 69 % with the air holes.

IV. Sensor Configuration

This section will explain the mAb sample preparation methods and the arrangement of the sensing system. The alignment process and a discussion of the coupling losses are presented. The section concludes with an overview of the sensor design and implementation.

A. Antibody Preparation

Commonly occurring human serum immunoglobulins, about 80 %, are IgG protein [1]. They are extensively studied antibodies. They are frequently detected as a response to pathogens. The ability to detect IgG would signify fast response detection technology for pathogens without having to isolate the pathogen, which typically requires long periods of incubation or costly laboratory infrastructure for molecular detection. The human IgG (UNLB) mAbs were supplied by Southern Biotechnology Associates, Inc. (Birmingham, AL). To conform to the characteristics of a standard reference reagent, and to ensure lot-to-lot consistency, each batch of mAbs is tested by ELISA methods before it is shipped from Southern Biotechnology Associates, Inc. The mAbs are from pooled normal human sera, purified by affinity chromatography on protein G covalently linked to agarose with a purity greater than 90 % [25]. Please note that although the antibodies employed in this study are from pooled normal human sera, in this article, the term monoclonal antibodies is defined in a broad sense to include antibodies containing a single antibody recognizing only a single determinant, i.e., antigen [1]. The mAbs are supplied in aqueous form with a concentration of 1 mol/mL. This concentration was diluted to 0.1 mol/mL to test the detection limits of the sensor. The dilution was performed via a recursive method. First, the mAbs are thoroughly homogenized via mechanical methods. A micropipette was used to collect 1 mL of the mAb preparation that was diluted with 9 mL of distilled water suitable for bioanalysis. This mixture yielded 10 mL of 0.1 mol/mL mAb solution. Both concentrated and diluted mAb preparations were stored at -20°C according to standard and supplier recommended storage methods. The samples were kept at a constant temperature between 2°and 8° C during the dilution and testing process for brief periods no longer than 10 minutes. No sample solutions were used after 1 week from the initial dilution to insure the quality of the tested samples.

B. Sensor Design

The SW-PCF mAb detector configuration presented in this article is a modified version of preliminary configurations [13], [14]. The detector is made up of a single mode fiber, butt-coupled to a 0.8 m length of SW-PCF. The two fibers are aligned using a 3-axis micropositioner so that the optical field guided in the single mode fiber is coupled into the solid silica core of the SW-PCF.

The fibers were butt-coupled in order to provide ease of access to the end of the SW-PCF so that the fluid can be inserted and removed from the fiber with ease. The SW-PCF provides a unique cross-section and several other advantages for antibody detection. The 3.3 μm core and 22 μm microstructure provide a large surface area for the coating of the fluid inside the fiber. The solid core waveguide confines the light so that the fluid inside the air holes can be detected via evanescent wave sensing. The aqueous mAb sample was inserted into the fiber by exploiting its capillary forces, as the small diameter air-holes of the structure forced the fluid into the fiber.

The other end of the SW-PCF was coupled to the spectrum analyzer. A simple cleaving of the filled tip of the fiber can be employed to ensure the complete removal of the sample from the SW-PCF.

C. Alignment

The alignment process requires a light source and an optical spectrum analyzer. The SW-PCF is placed on a fixed stage and coupled to the spectrum analyzer. A single mode fiber (See Fig. 2.) During the initial setup, a visible laser is used for visual alignment of the fiber. The fiber alignment was further optimized with an infrared laser source. A spectrum analyzer was used to detect the transmission through the aligned system with a broadband LED. Only minor adjustments were needed to achieve a peak in optical power around 0.3 μW at 1300 nm.

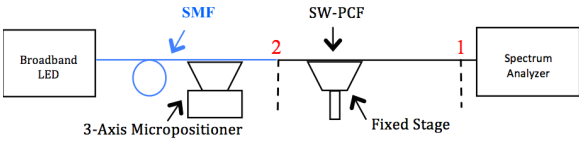

Fig. 2. Schematic of the sensor alignment process. The light sources employed during the alignment process are a visible laser, a infrared laser and broadband LED.

D. Coupling Losses

The detection system experiences several coupling losses, in addition to the conventional 3 dB per connector loss at the laser and spectrometer connections. The three main coupling losses faced were lateral misalignment losses, angular misalignment losses, and mode field diameter mismatch losses. The method by which the sensor was configured gives the most control over longitudinal alignment, hence longitudinal losses were negligible [26].

1) Lateral Misalignment: Lateral misalignment is an offset of the two fiber ends. It is best described as a radial offset where $r^2 = x^2 + y^2$ rather than an offset in x and y separately [12]. The loss in percentage of maximum power is

$$Loss = 1 - \exp\left(\frac{-x}{w_o}\right)^2 \quad (1)$$

where x is the misalignment and w_o is the mode field radius. The coupling is very sensitive to lateral misalignments. At a

0733-8724 (c) 2015 IEEE. Personal use is permitted, but republication/redistribution requires IEEE permission. See http://www.ieee.org/publications_standards/publications/rights/index.html for more information.

This article has been accepted for publication in a future issue of this journal, but has not been fully edited. Content may change prior to final publication. Citation information: DOI 10.1109/JLT.2016.2518921, Journal of Lightwave Technology

wavelength of 1300 nm with a mode field radius of 4.65 μm, a 1.5 μm displacement can cause a loss of around 11 %.

The lateral displacement measurement was mitigated during the alignment process. The horizontal and vertical displacement were imaged via a viewing system. Lateral displacement was estimated for a displacement of 2.03 μm, which is 35 % of the SMF core. The loss associated with this displacement is near 9.89 % of the total input power.

2) Angular Misalignment: Angular misalignment losses are functionally very similar to lateral misalignment [12]. The loss is described by

$$Loss = 1 - \exp\left(\frac{-n_0 \pi w_0}{\lambda}\sin(\theta)\right)^2 \quad (2)$$

where w_0 is the mode field radius, λ is the wavelength, θ is the angle of displacement n_0 is the index of the material outside the fiber, which in our case is air. For small angles, there is a high sensitivity to angular misalignments. An angular misalignment of 2° can lead to a loss of about 13 %.

Angular misalignment was difficult to control. SW-PCF is a novel optical fiber. The fiber geometry is unconventional. The SW-PCF has a smaller overall diameter, causing it to remain loose inside the connectors and V-grooves. This gap, caused a high probability of displacement within the connectors and V-grooves, in turn causing unavoidable angular displacement. The angular displacement was estimated to be around 4°. This angular displacement caused a loss of 15.39 % of the total input power.

3) Mode Field Diameter Mismatch: The mode field diameter mismatch losses due to the SW-PCF geometry also contributes to the coupling losses. The single mode and multimode fibers have different core diameters compared to the SW-PCF. This difference will cause a mismatched mode field diameter leading to coupling losses [12] described by

$$Loss = 1 - \frac{4}{\left(\frac{w_1}{w_2} + \frac{w_2}{w_1}\right)^2} \quad (3)$$

where w_1 and w_2 are the mode field diameters of the SMF and PCF fibers, respectively. If one of the cores is 50 % larger than the other, there will be a loss of 13 %.

The mode field diameter mismatch losses were mitigated by using a SMF core size that is comparable to the core size of the SW-PCF. Due to the novelty of the SW-PCF core geometry, an exact match of the core size was not commercially available. The SW-PCF with a core of 3.3 μm, coupled to a SMF with a core of 5.8 μm had a mismatch ratio of 1.75. This mismatch caused a 24 % loss of the total input power.

Fresnel reflection losses were also considered. This loss occurs at the joint of the butt coupled fibers due to the difference of refractive indices between the silica glass cores and the air gap between the coupled cores. Assuming normal incidence, the reflected power is given as $R = (n_1 - n_2)^2/(n_1 + n_2)^2$ where n_1 is the air (lower) refractive index and n_2 is the silica glass (higher) refractive index. The losses are typically 4% for a single air-glass interface. Yielding a nearly 16 % loss.The lateral-displacement losses, angular-displacement losses, mode field diameter mismatch losses and Fresnel losses detailed above, at 10 %, 15 %, 25 % and 16 % respectively, cause a nearly 65 % loss of the total input power.

V. Experiments and Results

The experiments involved measuring the transmittance of an empty fiber compared to a fiber filled with approximately 4.5 nL - 7.3 nL of 0.1 mol/mL mAb solution. The initial baseline reading of the LED spectrum between 1300 nm and 1700 nm was measured. The diluted 0.1 mol/mL mAb solution was thoroughly homogenized before each trial, to reduce the presence of bubbles or any other inconsistencies in the spectral absorption. The three 22 μm diameter air-holes, have an effective cross sectional area of 1.14 μm^2. A 2 cm length of the steering wheel photonic crystal fiber is immersed in the solution, allowing the capillary forces to fill 4.47 nL of the 0.1 mol/mL mAb stock solution into the cavities of the SW-PCF. The capillary filling process follows the Lucas-Washburn equation [4], [27]. This equation arises when a force balance relationship is considered between capillary and friction forces for ideal filling conditions producing a meniscus velocity for a constant contact angle. The Washburn equation describes the fluid mechanics of the filling dynamics for a capillary tube with a horizontal orientation. According to this equation the meniscus height, h, varies as $\sqrt{t}$ for a filling time, t (in seconds) and constant contact angle. The contact angle was determined for water at temperatures below 10°C. During the experiments, the mAb solution preparations for all four trials were maintained at a temperature between 2° and 8°C. Four different trials were performed to insure consistency and demonstrate repeatable sensor response. Trials 1 and 4 employed volumes of 7.31 nL at t= 8 s and 6.33 nL at t= 6 s, respectively. Both trials, the second and third, used a reduced sample volume of 4.47 nL for t= 3 s filling time.

A. Trial 1: mAb solution #1

In the first trial, after the baseline was recorded, the mAbs were inserted into the lattice of the SC-PCF from *position 1*, shown in Fig. 2. The SC-PCF was then coupled to the OSA and the output spectrum was measured. The absorption spectrum is calculated by subtracting the initial baseline from the mAb spectrum. The mAb absorption spectrum for the 7.31 nL sample is shown in Fig.3. The spectrum was determined by subtracting the mAb filled spectral signature from the empty fiber baseline at each wavelength point as

$$A = \sum_{\lambda=1300}^{\lambda=1700} A(\lambda) = \sum_{\lambda=1300}^{\lambda=1700} E(\lambda) - M(\lambda) \quad (4)$$

where A is the mAb absorption spectrum, $E(\lambda)$ and $M(\lambda)$ are the empty fiber and mAb filled fiber transmission spectra, respectively. Figure 3 shows the two absorption peaks of the mAb solution at 1435 nm and at 1530 nm with an absorption power of 1.55 nW and 3.2 nW, respectively.

0733-8724 (c) 2015 IEEE. Personal use is permitted, but republication/redistribution requires IEEE permission. See http://www.ieee.org/publications_standards/publications/rights/index.html for more information.

This article has been accepted for publication in a future issue of this journal, but has not been fully edited. Content may change prior to final publication. Citation information: DOI 10.1109/JLT.2016.2518921, Journal of Lightwave Technology

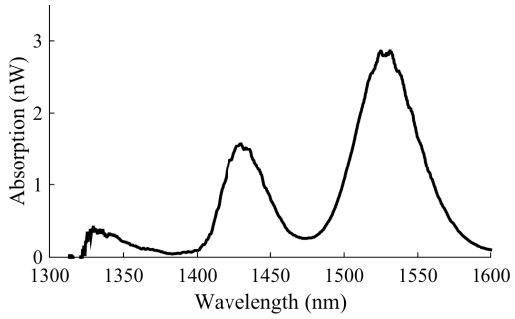

Fig. 3. Absorption signature of trial 1 results of a 7.31 nL mAb sample filled SW-PCF.

B. Trial 2: mAb solution #2

In the second trial, the freshly prepared sample of 0.1 mol/mL mAb solution was inserted into *position 1* of the SW-PCF. The mAbs were then inserted inside the lattice of the SW-PCF, and the first trial experiment was repeated. The spectral signature shows a consistency of location and relative power, in spite of the realignment process and different batches of diluted mAb solution.

The absorption spectrum in Fig. 4 for the second trial was determined according to (4). The butt coupled fibers formed an optical cavity which led to unwanted Fabry-Perot effects. These effects appear as oscillations at intermediate wavelengths in the absorption spectra. In the second trial, the interferences (ripples) were especially pronounced. It should be noted that, during the second trial, construction work was in progress on site. The presence of the low frequency vibrations in the readings shown in Fig. 4 as ripples between 1520 nm and 1575 nm are evidence of the event. However, the uniformity of the spectral signature peaks persisted. This interference due to mechanical vibrations affecting the butt coupling of the fibers was significant. These unwanted effects can be resolved by employing an angle polished fiber or modified alignment. The spectral measurements were repeated for the same sample volume in the third trial.

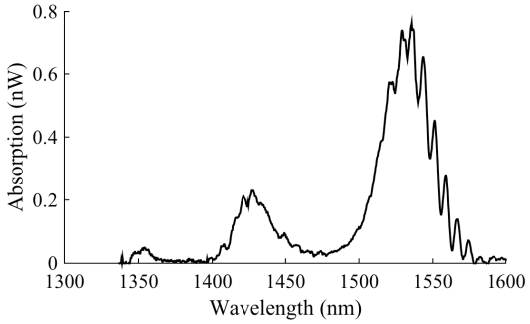

Fig. 4. Absorption signature of trial 2 results of a mAb filled SW-PCF.

The results were consistent between the first and second trials. In addition, it showed that modifications to the sensor configuration or insertion methods would enhance the magnitude of the absorption and would not alter the absorption spectral signature.

C. Trial 3: mAb solution #3

In the third trial, the insertion position of the mAb solution was changed to test if the position of the solution inside the SW-PCF relative to the light source and the spectrum analyzer would lead to any anomalies. The mAb solution was inserted from the *position 2* location, making it closer to the broadband light source and farther from the spectrum analyzer.

Figure 5 shows the absorption spectrum according to (4). The transmission power for the third trial measurements was higher than the second trial while the absorption strengths remained consistent through the three trials. The spectrum for the third trial agrees with the results from the first and second trials for the 1440 nm and 1530 nm absorption peaks of the mAb solution.

D. Trial 4: mAb solution #4

In the fourth trial the solution was inserted into the *position 2* location but the SW-PCF was immersed in the mAb solution for 6 seconds allowing the capillary forces [28] to increase the solution volume entering into the SW-PCF lattice to 6.33 nL.

Figure 5 shows that the results were consistent for a larger volume of solution 6.33 nL. The absorption peaks were observed in the 1400 nm to 1475 nm range and in the 1500 nm to 1575 nm range. The magnitude of the maximum absorption increased. The relative maximum absorption ratio of the two peaks demonstrated a consistent mAb absorption spectral signature throughout the trials.

E. Analysis

In all four trials, the mAbs exhibited spectral absorbance in two ranges, between the wavelengths 1400 nm and 1450 nm and between 1500 nm and 1550 nm. These experiments included a negative control, the buffer solution used for dilution of the mAb samples. These spectral signatures were uniquely different from the spectral measurements of the buffer solution demonstrating that the sensor is specific. Figure 5 shows the absorption spectra of all four trials. The spectra absorbances are consistent with the Beer-Lambert principle discussed in section II. The strongest absorbance corresponds to the 7.31nL sample with an interaction length of 6.31 mm. This absorbance is linearly proportional to the absorbance for the 4.47 nL and 6.3 nL samples volumes with interaction lengths of 3.9 mm and 5.5 mm, respectively. The sensitivity of the SW-PCF-based sensor depends on the interaction length [4]. The featured experimental configuration is able to detect down to pW absorption power levels. The maximum sensitivity for the proposed sensor with a 4.5 nL sample volume is 76 mmol/ml. For a fiber length of 80 cm the minimum detection concentration possible is 0.37 mmol/mL.

The light source used in the experiments was a broadband LED. The output spectrum of the broadband LED is not

0733-8724 (c) 2015 IEEE. Personal use is permitted, but republication/redistribution requires IEEE permission. See http://www.ieee.org/publications_standards/publications/rights/index.html for more information.

This article has been accepted for publication in a future issue of this journal, but has not been fully edited. Content may change prior to final publication. Citation information: DOI 10.1109/JLT.2016.2518921, Journal of Lightwave Technology

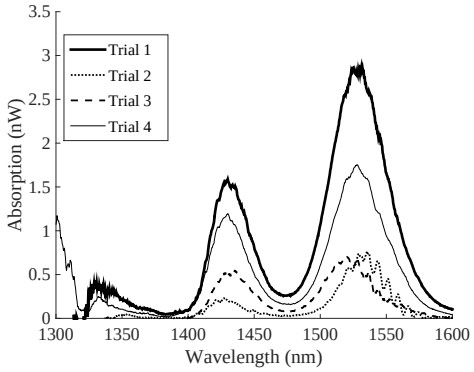

Fig. 5. A comparison of the absorption spectra for the four trials is shown. The absorbance of the four samples are linearly proportional and are consistent with the Beer-Lambert principle.

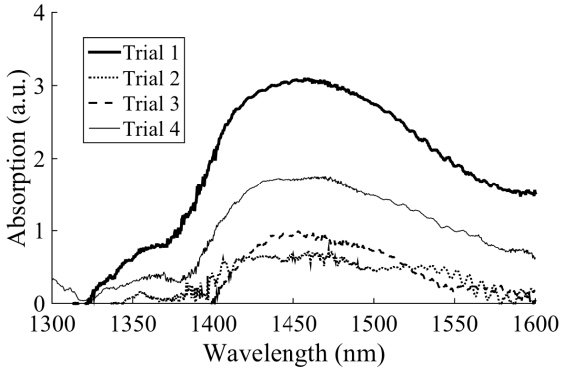

Fig. 6. A comparison of the processed mAb spectra is shown.

flat. The LED light source emits four equally spaced emission peaks. The spectral output of the LED was normalized and flattened with a filtering algorithm producing a set of weights that were used to flatten the LED spectrum. These weights were applied to the measured absorption spectra. The processed spectral output shown in Fig.6 agrees with the presented analysis. The observed filtered absorption levels are proportional with the experimental results.

The performed experiments show a consistency of the spectral signature of the mAb absorption, in maintaining the peak position and relative power levels, independent of the mAb loading procedure.

The trials exhibited maximum absorption at the ranges of 1400 nm to 1475 nm and 1500 nm to 1575 nm. In addition, the mAb samples exhibited emission at a wavelength of 1300 nm. The emission spectrum of the mAb solution presented a consistent spectral signature with a difference in peaks proportional to that of the absorption spectral signature. The emission observed at the 1300 nm wavelengths was unexpected, even though it is relatively weak. The emission is consistent with the background fluorescence generated by impurities in the glass [5].

The mAb absorption spectra are plotted in Fig. 6. The spectral signature of water was obtained from the HITRAN database [29]. When the mAb spectrum is compared to the absorption spectrum of water, the absorption of the mAb solution extends beyond the water signature range. The higher order peaks of the mAb solution, between 1400 nm and 1475 nm and between 1500 nm and 1575 nm, with line widths of 55 nm and 100 nm respectively, lay in a different range than that of water. The comparison in Fig. 6 shows that the higher order peaks are a strong indicator that the absorption is that of the mAb sample, and not of the diluting solution. The peaks of the water spectrum coincide with the first peak in the 1350 nm to 1370 nm range of the mAb absorption signature, suggesting that the first peak of the measured spectrum belongs to the water absorption.

VI. Conclusion

The significance of these results is that label-free detection of monoclonal antibodies has been demonstrated in the near infrared region with conventional light sources and detectors. The experimental results demonstrated that monoclonal antibodies absorb light at the indicated wavelengths. This provides a potential cost-effective alternative to environmental monitoring tools. This work demonstrates that the detection of antibodies using a solid core photonic crystal fiber in the 1300 nm to 1700 nm range is possible. The achieved results for the mAb samples diluted in pure water were encouraging and should promote future optical fiber based environmental and biological monitors.

An 0.8 m solid core photonic crystal fiber with a broadband LED and a conventional optical spectrum analyzer can be used to monitor mAbs. The maximum sensitivity for the proposed sensor (with pW level capabilities) for a 4.5 nL sample volume is 76 mmol/mL. For a fiber length of 80 cm with a 89 μL sample, the minimum detection concentration possible is 0.37 mmol/mL. The mAb absorption was detected in the window of 1300 nm to 1700 nm with only 4.47 nL of 0.1 mol/mL mAb solution. The sensor response time was less than 25 s, reducing detection time compared to common detection methods. The response time was limited by the scanning rate of the frequency selective elements of the spectrum analyzer. This response time can be reduced.

The mAb solution exhibited two distinct absorption peaks, a water linked absorption peak between 1400 nm and 1470 nm, with a maximum power of 1.65 nW, and a mAb linked absorption peak between 1485 nm and 1590 nm with a maximum power of 3.2 nW. In addition, the mAbs exhibited emission at wavelengths below 1350 nm, with a maximum emission power of 0.8 nW. The emission was proportional to the absorption. The experiments that showed the maximum absorption, exhibited the most emission and similarly for the intermediate and weak absorption profiles.

Trials 1 through 4 demonstrated that the position of the mAbs relative to the light source and to the spectrum analyzer had no effect on the shape of the absorption spectrum; rather the position only affected the magnitude of the absorption. In addition, the volume of the sample is also irrelevant to the

0733-8724 (c) 2015 IEEE. Personal use is permitted, but republication/redistribution requires IEEE permission. See http://www.ieee.org/publications_standards/publications/rights/index.html for more information.

This article has been accepted for publication in a future issue of this journal, but has not been fully edited. Content may change prior to final publication. Citation information: DOI 10.1109/JLT.2016.2518921, Journal of Lightwave Technology

spectral signature, where samples with a volume of 4.47 nL and 6.33 nL resulted with absorption at the same wavelength, with the same shape, but with magnitudes proportional to the mAb sample volume.

ACKNOWLEDGMENT

The authors would like to thank Dr. Henry Du at the Chemical Engineering and Materials Science Department at Stevens Institute of Technology for providing SC-PCF samples.

REFERENCES

[1] M. T. Madigan, J. M. Martinko, and T. D. Brock, *Brock biology of microorganisms*. Upper Saddle River, NJ: Pearson Prentice Hall, 2006, pp. 744–796.

[2] D. Wild, Ed., *The Immunoassay Handbook, Theory and applications of ligand binding, ELISA and related techniques*. Elsevier Science, February 2013, ch. 2, pp. 203–204.

[3] S. C. Warren-Smith, G. Nie, E. P. Schartner, L. A. Salamonsen, and T. M. Monro, "Enzyme activity assays within microstructured optical fibers enabled by automated alignment," *Biomed. Opt. Express*, vol. 3, no. 12, pp. 3304–3313, Dec 2012. [Online]. Available: http://www.osapublishing.org/boe/abstract.cfm?URI=boe-3-12-3304

[4] L. H. P. Jesper B. Jensen, "Photonic crystal fiber based evanescent-wave sensor for detection of biomolecules in aqueous solutions," *Optics Letters*, vol. 29, no. 17, pp. 1974–1976, 2004.

[5] Y. Ruan, E. P. Schartner, H. Ebendorff-Heidepriem, P. Hoffmann, and T. M. Monro, "Detection of quantum-dot labelled proteins using soft glass microstructured optical fibers," *Opt. Express*, vol. 15, no. 26, pp. 17 819–17 826, Dec 2007. [Online]. Available: http://www.opticsexpress.org/abstract.cfm?URI=oe-15-26-17819

[6] S. Padmanabhan, V. K. Shinoj, V. M. Murukeshan, and P. Padmanabhan, "Highly sensitive optical detection of specific protein in breast cancer cells using microstructured fiber in extremely low sample volume," *Journal of Biomedical Optics*, vol. 15, no. 1, pp. 017 005–017 005–6, 2010. [Online]. Available: http://dx.doi.org/10.1117/1.3302810

[7] T. M. Monro, S. Warren-Smith, E. P. Schartner, A. François, S. Heng, H. Ebendorff-Heidepriem, and S. A. V, "Sensing with suspended-core optical fibers," *Optical Fiber Technology*, vol. 16, no. 6, pp. 343 – 356, 2010, special Fiber Structures and their Applications. [Online]. Available: http://www.sciencedirect.com/science/article/pii/S1068520010000878

[8] T. Monro, H. Ebendorff-Heidepriem, E. Schartner, and S. Warren-Smith, "Sensing in suspended-core optical fibers," in *Winter Topicals (WTM), 2011 IEEE*, Jan 2011, pp. 159–160.

[9] E. P. Schartner, G. Tsiminis, A. François, R. Kostecki, S. C. Warren-Smith, L. V. Nguyen, S. Heng, T. Reynolds, E. Klantsataya, K. J. Rowland, A. D. Abell, H. Ebendorff-Heidepriem, and T. M. Monro, "Taming the light in microstructured optical fibers for sensing," *International Journal of Applied Glass Science*, vol. 6, no. 3, pp. 229–239, 2015. [Online]. Available: http://dx.doi.org/10.1111/ijag.12128

[10] C. Markos and O. Bang, "Nonlinear label-free biosensing with high sensitivity using as2s3 chalcogenide tapered fiber," *Lightwave Technology, Journal of*, vol. 33, no. 13, pp. 2892–2898, July 2015.

[11] C. Markos, W. Yuan, K. Vlachos, G. E. Town, and O. Bang, "Label-free biosensing with high sensitivity in dual-core microstructured polymer optical fibers," *Opt. Express*, vol. 19, no. 8, pp. 7790–7798, Apr 2011. [Online]. Available: http://www.opticsexpress.org/abstract.cfm?URI=oe-19-8-7790

[12] W. Demtröder, *Laser Spectroscopy: Basic Concepts and Instrumentation*, 2nd ed. Springer, 1996.

[13] E. Battinelli, F. Anuszewski, M. Reimlinger, W. Kelly, and R. Wynne, "Steering wheel photonic crystal fiber for monoclonal antibody detection," in *Sensors, 2011 IEEE*, Oct 2011, pp. 1921–1924.

[14] J. DellAntonio, N. Giambrone, F. Anuszewski, R. Wynne, and W. Kelly, "Enzyme-linked monoclonal antibody microstructured optical fiber monitor," in *Proc. SPIE*, vol. 8693, 2013, pp. 86 930U–86 930U–8. [Online]. Available: http://dx.doi.org/10.1117/12.2009509

[15] J. M. Hollas, *Modern Spectroscopy*, Chichester, Ed. Wiley, 2004.

[16] M. D. B. Daniel C. Harris, *Symmetry and Spectroscopy: An Introduction to Vibrational and Electronic Spectroscopy*, ser. Dover Books on Chemistry. Dover Publications, November 1989.

[17] P. F. Bernath, *Spectra of Atoms and Molecules*, 2nd ed. New York, NY: Oxford University Press, 2005.

[18] P. Vadillo, *Laser Diode Gas Spectroscopy*. Intech Open Access Publisher, 2012.

[19] R. M. Measures, *Laser Remote Chemical Analysis*. New York, NY: John Wiley and Sons, Inc., 1988, vol. 94.

[20] O. Svelto, *Principles of Lasers*, 5th ed. Springer, 2010.

[21] M. Lepere, "Line profile study with tunable diode laser spectrometers," *Spectrochimica Acta Part A: Mplecular and Biomolecular Spectroscopy*, vol. 60, no. 14, pp. 3249–3258, December 2004.

[22] P. L. Varghese and R. K. Hanson, "Collisional narrowing effects on spectral line shapes measured at high resolution," *Applied Optics*, vol. 23, no. 14, pp. 2376–2385, 1984.

[23] Y. Zhu, R. T. Bise, J. Kanka, P. Peterka, and H. Du, "Fabrication and characterization of solid-core photonic crystal fiber with steering- wheel air-cladding for strong evanescent field overlap," *Optics Communications*, vol. 281, no. 1, pp. 55–60, January 2008.

[24] J. Rabah, A. Mansaray, R. Wynne, and M. Duran, "Steering wheel photonic crystal fiber for human igg detection," in *SENSORS, 2014 IEEE*. SENSORS, 2014 IEEE, November 2014.

[25] I. Southern Biotechnology Associates, "Technical notes: Human igg isotype control," Southern Biotechnology Associates, Inc., 160 Oxmoor Blvd, Birmingham, AL 35209 USA, Tech. Rep. TB0150, March 2015.

[26] European, Radiocommunications, Committee, and (ERC), "A comparison of the minimum coupling loss method, enhanced minimum coupling loss method, and the monte-carlo simulation," European conference of postal and telecommunications administrations, Menton, Tech. Rep., 1999.

[27] M. Stange, M. E. Dreyer, and H. J. Rath, "Capillary driven flow in circular cylindrical tubes," *Physics of Fluids*, vol. 15, no. 9, pp. 2587–2601, 2003.

[28] E. W. Washburn, "The dynamics of capillary flow," *Phys. Rev.*, vol. 17, no. 3, pp. 273–283, March 1921.

[29] L. Rothman, "The hitran2012 molecular spectroscopic database, journal of quantitative spectroscopy and radiative transfer," *Journal of Quantitative Spectroscopy and Radiative Transfer*, vol. 130, pp. 4–50, 2013.

Rosalind Wynne is an Associate Professor at Villanova University in the Department of Electrical and Computer Engineering. Dr. Wynne received her doctorate in Electrical Engineering from Boston University (2005), a M.S. in Electrical Engineering from Boston University (2001) and a B.S. in Physics from Norfolk State University (1999). She is a member of the International Society for Optical Engineering (SPIE), the Institute of Electrical and Electronics Engineers (IEEE) and the National Society of Black Engineers (NSBE).

Jad Rabah is a graduate student (M.S.E.E. 2015) at Villanova University.

Alpha Mansaray is an undergraduate student (B.S.M.E. 2015) at Villanova University.

Metin Duran is a Professor in the Civil and Environmental Engineering Department at Villanova University.

0733-8724 (c) 2015 IEEE. Personal use is permitted, but republication/redistribution requires IEEE permission. See http://www.ieee.org/publications_standards/publications/rights/index.html for more information.